Published in final edited form as:
J Med Chem. 2012 November 26; 55(22): 9549–9561. doi:10.1021/jm3008079.

Variation of the net charge, lipophilicity and side chain flexibility in Dmt[1]-DALDA: effect on opioid activity and biodistribution

Alexandre Novoa[1], **Sylvia Van Dorpe**[2], **Evelien Wynendaele**[2], **Mariana Spetea**[3], **Nathalie Bracke**[2], **Sofie Stalmans**[2], **Cecilia Betti**[1], **Nga N. Chung**[4], **Carole Lemieux**[4], **Johannes Zuegg**[5], **Matthew A. Cooper**[5], **Dirk Tourwé**[1], **Bart De Spiegeleer**[2,*], **Peter W. Schiller**[4], and **Steven Ballet**[1,*]

[1]Department of Organic Chemistry, Vrije Universiteit Brussel, Pleinlaan 2, B-1050, Brussels, Belgium

[2] Drug Quality and Registration (DruQuaR) Group, Department of Pharmaceutical Sciences, Ghent University, Ghent, Belgium

[3]Department of Pharmaceutical Chemistry, Institute of Pharmacy and Center for Molecular Biosciences Innsbruck (CMBI), University of Innsbruck, Innsbruck, Austria

[4]Laboratory of Chemical Biology and Peptide Research, Clinical Research Institute of Montreal, Montreal, QC, Canada

[5]Institute for Molecular Bioscience, University of Queensland, Brisbane, Australia.

Abstract

The influence of the side chain charges of the second and fourth amino acid residues in the peptidic μ opioid lead agonist Dmt-D-Arg-Phe-Lys-NH_2 ([Dmt[1]]-DALDA) was examined. Additionally, to increase the overall lipophilicity of [Dmt[1]]-DALDA and to investigate the Phe[3] side chain flexibility, the final amide bond was *N*-methylated and Phe[3] was replaced by a constrained aminobenzazepine analogue. The *in vitro* receptor binding and activity of the peptides, as well as their *in vivo* transport (brain in- and efflux and tissue biodistribution) and antinociceptive properties after peripheral administration (i.p. and s.c.) in mice were determined. The structural modifications result in significant shifts of receptor binding, activity and transport properties. Strikingly, while [Dmt[1]]-DALDA and its *N*-methyl analogue, Dmt-D-Arg-Phe-*N*MeLys-NH_2, showed a long-lasting antinociceptive effect (>7h), the peptides with D-Cit[2] generate potent antinociception more rapidly (maximal effect at 1h post-injection) but also lose their analgesic activity faster, when compared to [Dmt[1]]-DALDA and [Dmt[1],*N*MeLys[4]]-DALDA.

Introduction

Due to the present limitations of the pharmacotherapy of pain, the development of novel medications for the treatment of severe and chronic pain represents a high priority goal. To date, these pathologies rely mostly on opioid analgesics, but the current available opioid drugs produce a number of side-effects that limit their clinical use. A considerable amount

[*]***Corresponding Authors:*** Steven Ballet, Organic Chemistry Department, Vrije Universiteit Brussel, Pleinlaan 2, B-1050 Brussels, Belgium, phone +32 2 6293292, sballet@vub.ac.be; Bart De Spiegeleer, Drug Quality and Registration (DruQuaR) Group, Faculty of Pharmaceutical Sciences, Ghent University, Harelbekestraat 72, B-9000 Ghent, Belgium, phone +32 9 2648100, bart.despiegeleer@ugent.be. .

Supporting Information Available: Characterization of non-key compounds, ED_{50} values of selected peptides and morphine at different time points after s.c. administration, and Caco-2 cell permeability data. This material is available free of charge via the internet at http://pubs.acs.org.

of work has been done and is still needed to target more efficacious and non-addicting analgesics in order to solve this major health care problem. One research avenue consists of the discovery and development of a potent peptide-based analgesic, with reduced undesired effects, requiring a compound with a high affinity for μ and/or δ opioid receptors (MOR and DOR, resp.), a potent *in vitro* agonist activity, a strong antinociceptive effect *in vivo*, an improved resistance to enzymatic degradation and the ability to cross the blood-brain barrier (BBB), allowing systemic administration. More specifically, it was evidenced that compounds with a dual MOR/DOR activity present beneficial pharmacological effects in comparison to highly selective MOR agonists. There have been reports on synergistic effects between MOR agonists and DOR agonists.[1,2] Therefore, compounds with a mixed μ agonist/δ agonist profile have the potential to be effective for the treatment of pain with reduced side effects, as lower doses would be required.[3] In parallel to the development of such dual agonists, mixed MOR agonists/DOR antagonists were also designed in search of a better pain management.[4-6] Among other beneficial effects, the observation that the selective blockade of DOR suppressed morphine tolerance and dependence motivated the development of compounds with this mixed profile.[7]

Earlier studies, performed by Schiller and coworkers,[8] on the dermorphin (H-Tyr-D-Ala-Phe-Gly-Tyr-Pro-Ser-NH_2)-derived tetrapeptide H-Dmt-D-Arg-Phe-Lys-NH_2 **1** ([Dmt[1]]DALDA, Figure 1), identified this peptide as a highly potent MOR agonist with a high binding affinity at the MOR (K_i^{μ} = 0.143 nM, 7-fold higher than morphine) and a high metabolic stability, when incubated in sheep blood ($t_{1/2}$ = 1.8 h).[9] The C-terminal amidation and insertion of a D-Arg residue in position 2 are likely to assist in the high stability of this peptide.[9] Moreover, [Dmt[1]]DALDA showed extraordinary potency in the rat tail-flick assay after intrathecal administration (3000 times more potent than morphine),[10] and a subcutaneous (s.c.) administration also induced a potent analgesic response,[11,12] which in turn indicated that this molecule is able to cross the BBB. Nevertheless, the structural features of this tri-charged peptide responsible for its ability to cross the BBB have not clearly been determined.

The introduction of a conformational constraint and the *N*-methylation of peptidic amide bonds are well-known procedures to improve the stability and the activity of (opioid) peptides.[13,14] Previously, we have used the 4-amino-1,2,4,5-tetrahydro-2-benzazepin-3-one (Aba) scaffold **2** (Figure 1) as a tool for introducing a local conformational constraint in opioid peptides.[15-19] The synthetic Aba residue can be considered as a constrained phenylalanine where the phenyl group is fixed to the amine of the next amino acid via a methylene bridge.[17] Previous work on opioid peptides indicated that replacement of Phe by Aba in dermorphin-based sequences improves the DOR affinity considerably, while preserving the binding to the MOR.[17,18] Additionally, peptides containing this constraint represent highly active antinociceptive agents when tested *in vivo*, as recently reported.[19] Similarly, amide *N*-methylation in opioid peptide sequences have shown to result in retained opioid receptor binding and activation,[20] as well as improved BBB passage[21] when compared to the non-methylated analogues. Therefore, both conformational side chain restriction and *N*-methylation prove to be efficient techniques in improving the pharmacokinetic and pharmacodynamic profile of dual MOR/DOR opioid peptides.[22]

The present work describes the chemical modification of the MOR lead tetrapeptide [Dmt[1]]DALDA (Figure 1). The different modifications that were carried out comprise: i) changing the overall net charge in the peptide by replacing the D-Arg[2] residue by a D-Cit[2] and/or the Lys[4] residue by a Nle[4], ii) the introduction of a *N*-methyl group in the amide bond connecting residues in position 3 and 4, in order to protect the peptide against enzymatic degradation and to increase the overall lipophilicity of the peptide, and iii) introducing a conformational constraint by means of an Aba[3] residue that replaces Phe[3] in

the Dmt[1][DALDA] sequence. The synthesized peptides have been investigated for their opioid receptor binding affinity and agonist potency, BBB permeability, plasma stability and antinociceptive activities. Structure-activity relationship (SAR) studies relating to the substitution pattern in targeted positions within this series were pursued.

Results and discussion

Synthesis

All standard and *N*-methylated amino acids were obtained from commercial sources, whereas the conformationally constrained aminobenzazepinones of type **2** were prepared as described below, and used in standard solid phase peptide synthesis.

1. Synthesis of the 4-amino-2-benzazepin-3-one scaffolds

The preparation of the required Aba-Lys/Nle dipeptidomimetics **8a**,**b** was performed using a previously reported[23] and optimized procedure[24] (Scheme 1). The phthaloyl-protected (*S*)-*o*-cyano-phenylalanine **3**, was obtained by reaction of methyl 2-[(succinimidooxy)-carbonyl]benzoate[25] with the commercially available *o*-(*S*)-cyanophenylalanine. The corresponding *o*-formyl intermediate **4** was formed by hydrogenation with Raney Nickel in an acetic acid/water/pyridine mixture. Reductive amination of **4** with lysine and norleucine amino acid methyl esters resulted in secondary amines **5a/b**, which were subsequently used for the dicyclohexylcarbodiimide-induced ring closure to present the desired aminobenzazepinones **6a/b**. Ester hydrolysis, followed by phthaloyl-removal with hydrazine hydrate and final Fmoc-protection gave the required Fmoc-Aba-Lys(Z)/Nle-OH building blocks **8a/b** which were used in the peptide synthesis.

2. Peptide synthesis

The peptides in this study were synthesized manually using N^{α}-Fmoc- or N^{α}-Boc-protected amino acids on Rink amide resin (0.31 mmol scale) and MBHA resin (0.29 mmol scale) using DIC and 1-hydroxybenzotriazole (HOBt) or *O*-(benzotriazol-1-yl)-*N,N,N',N'*-tetramethyluronium tetrafluoroborate (TBTU)/*N,N*-diisopropylethylamine (DIPEA) as the coupling reagents/mixtures. A threefold excess of the building blocks (Fmoc-Aba-Lys(Z)-OH, Fmoc-Aba-Nle-OH, Fmoc-Lys(Boc)-OH, Boc-Lys(Z)-OH, Boc-*N*MeLys(Z)-OH, Fmoc-Nle-OH, Boc-*N*MeNle-OH, Fmoc- or Boc-Phe-OH, Fmoc-D-Arg(Pbf)-OH, Boc-D-Arg(Tos)-OH, Boc-D-Cit-OH and Boc-Dmt-OH) and activating agents was applied and dry DMF was used as a solvent. Fmoc-deprotections were carried out by treating the resin twice (5 min and 15 min) with 20% piperidine in DMF. Boc-Dmt-OH was used in a final coupling, to directly present the fully unprotected peptide after acidic cleavage from the resin. Boc-Dmt-OH was coupled with 1,3-diisopropylcarbodiimide (DIC) and HOBt in order to avoid side reactions when uronium-based coupling reagents were used. Final cleavage of the peptide as well as the 2,2,4,6,7-pentamethyldihydrobenzofuran-5-sulfonyl (Pbf) side chain protection group removal was accomplished by treatment with TFA/CH_2Cl_2/anisol 90:5:5 for 90 min (Rink resin) or standard HF/anisol cleavage conditions for 60 min (MBHA resin). The crude peptides were obtained after evaporation of the cleavage mixture, precipitation in cold Et_2O, dissolving in glacial acetic acid and subsequent lyophilization. Final purification was performed by RP-HPLC on a SUPELCO DiscoveryBIO wide pore preparative C18 column in 45% overall yield and was >95% pure as determined by analytical RP-HPLC. The structures of the compounds were confirmed by high-resolution electrospray (ESP) ionization mass-spectrometry.

Biological evaluation and structure-activity relationships

***In vitro* opioid receptor binding and activity (Table 1)—**The investigated peptides can be subdivided in three series: i) peptides **1** and **9** to **11** in which the side chain charges were altered, ii) the analogous series where the α-amine of the C-terminal residue is methylated (peptides **12** to **15**) and iii) the tetrapeptides with restricted side chain flexibility after a $Phe^3 \rightarrow Aba^3$ substitution (compounds **16** to **19**). Peptide **20** (Dmt-D-Arg-Aba-Gly-NH_2) was reported recently,[19] but is included in this work as a reference compound.

In general, the replacement of $D\text{-}Arg^2$ in the H-Dmt-D-Arg-Phe-Lys-NH_2 analogues by $D\text{-}Cit^2$ preserves the low- to subnanomolar MOR binding affinity, produces shifts in κ opioid receptor (KOR) binding, and enhances the DOR affinity in most cases (except for **18** vs. **16**). This MOR/DOR selectivity shift is in agreement with the *in vitro* functional activities at both receptor types, as indicated by the results of the guinea pig ileum (GPI) and mouse vas deferens (MVD) bioassays. Structurally, D-Cit resembles D-Arg but it is not charged at physiological pH. The binding and activation of MOR and DOR confirms that the charge of the guanidinium moiety in $D\text{-}Arg^2$ is not crucial for receptor recognition, being in line with earlier findings of other opioid peptides such as, for example, the dermorphin, endomorphin and enkephalin peptides that bear respectively a D-Ala, Pro or Gly residue in position 2. Similarly, the side chain charge of the Lys residue in position 4 was removed via replacement with Nle, a residue that lacks the terminal amino group in the side chain. As shown in Table 1, this modification did not markedly affect the interaction with the MOR receptor, but produced a significant 55- (**1** vs. **9**), 19- (**12** vs. **13**) and 5- fold (**16** vs. **17**) improvement of both DOR binding and *in vitro* functional activity [4- (**1** vs. **9**), 5- (**12** vs. **13**) and 21- fold (**16** (IC_{25}) vs. **17**)]. In this case, the favorable interaction with DOR may be a result of not only the absence of a side chain charge, but also other factors like hydrogen bonding or steric effects (amine function vs. hydrogen) have to be considered. In respect to the KOR affinity, the $Lys^4 \rightarrow Nle^4$ substitution slightly improves binding when $D\text{-}Arg^2$ is preserved (**1** vs. **9** and **12** vs. **13**). However, when combined with the $D\text{-}Arg^2 \rightarrow D\text{-}Cit^2$ modification, a significant loss of KOR affinity is observed.

Previously, we have shown that constraining the conformation of Phe^3 in dermorphin-derived tetrapeptides into a 4-amino-tetrahydro-2-benzazepin-3-one ring **2** leads to highly potent peptides.[18,19] To distinguish the influence of the ring constraint from that of the *N*-alkylation of the Gly^4 residue, the "ring opened" analogs containing an amide N-methylation were prepared, and were shown to be of equal potency.[21] Therefore, the *N*-methylated Lys^4 analogues of Dmt^1-DALDA were now also investigated. The *N*-methylation of the Xxx^3-Yyy^4 amide bond, on the other hand, influences the cis-trans isomer equilibrium of the peptide bond between these amino acids and stabilizes this bond against enzymatic degradation, but also increases the overall lipophilicity of the peptide analogues. Clearly, when comparing the peptides of the first series (peptides **1** and **9** to **11**) with the respective peptide analogues of the second series (**12** to **15**), the receptor binding data were very similar, whereas the functional GPI and MVD assays gave values slightly in disfavor of MOR activation, but in favor of DOR activity.

In contrast to the first eight analogues in Table 1, for which high MOR and DOR receptor binding and potent opioid activity are obtained, the next analogues including the conformationally constrained Aba-Lys dipeptide (**16** and **17**), presented in vitro activity data with more pronounced shifts. When Aba^3-Lys^4 was inserted in the peptide (**16**), the MOR affinity was retained, but the DOR affinity increased by a factor 23, in agreement with previous findings.[18] However, the ability to activate MOR and DOR decreased substantially. Because of this drop in activity, we did not perform any further KOR binding studies for compounds **16** and **18**. The ability of DOR activation was restored in the Nle^4 analogue **17**

and concomitantly improved KOR binding considerably (IC_{50} ≈ 1.12 nM). A combination of D-Cit[2] and Aba[3]-Nle[4] substitutions in **19** resulted in the conversion of the potent MOR selective Dmt[1]-DALDA **1** into a potent non-selective MOR partial agonist/DOR full agonist **19**.

Previously, the opioid sequence Dmt[1]-D-Arg[2]-Aba[3]-Gly[4]-NH_2 **20** was identified as a potent antinociceptive opioid peptide.[19] The present data showed that the constrained amino-azepinone scaffold should not be used in opioid tetrapeptides in combination with a Lys[4] amino acid, but preferably in combination with a Gly[4] residue, when aiming at combined MOR/DOR agonists.

Brain influx and efflux—Determination of the blood-brain barrier transport properties (initial influx K_{in}, V_{br}, brain capillary and parenchyma fraction and efflux k_{out}) form important parameters to determine the "druggability" of central nervous system (CNS)-compounds. Therefore, the transport properties of the peptides **1**, **9**, **10**, **12**, **14** and **20** were determined in CD-1 mice. After labeling with ^{125}I, the radiolabeled peptides were injected into the jugular vein and at specified time points after injection, the mice were decapitated and the brain was isolated for analysis (Table 2). These data clearly indicate an influx into the mouse brain for all peptides: peptides **12**, **10**, **20** and **14** show the highest initial K_{in} values, indicating a rapid and high influx of the radiolabelled peptides into the brain, while peptides **9** and **1** demonstrate slower influx properties. Moreover, the apparent brain distribution volumes, obtained from 15 min time interval and calculated according to Gjedde,[26] indicate relative high values of 27 μl/g, compared to 15 μl/g for the negative control Bovine serum albumin (BSA). Based on the capillary depletion results, a higher parenchyma versus capillary distribution for all peptides is observed: the amount of peptide entering the brain is mostly transferred from the capillaries to the parenchyma. This is in accordance with previous distribution results of other opioid peptides.[27] However, despite the good brain influx properties of peptide **20**, the net effect is expected to be reduced due to the significant brain to blood efflux transport. Also peptide **1** shows a non-negligible efflux, while this is less observed for peptides **10** and **12**, and not at all for peptides **9** and **14**.

Additionally, and in an effort to predict and potentially rank the ability of the peptides to permeate the BBB via use of an *in vitro* test, all compounds were subjected to a Caco-2 permeability assay (Supporting information). Very low peptide transport values through the Caco-2 cell monolayers (in both directions, *i.e.* apical→basal (A-B) and basal→apical (B-A)) were observed. However, a positive observation that was made from this study consisted of a low B-A transport, which is indicative of not hitting p-glycoprotein, an important efflux transporter that is present at high concentration in the luminal membrane of the brain endothelia.

***In vivo* tissue biodistribution—**Immediately after brain dissection, the spleen, liver, lungs, heart and kidneys were collected, the tissues were weighed, and the amount of radioactivity was measured. For each tissue, the percentage of mass-corrected injected dose (ID) was then calculated as described in the experimental section. The tissue distribution plots (Figure 2) show a strikingly high liver accumulation for peptide **9** as a consequence of the Lys[4] replacement by Nle[4]. Also for peptide **10**, a high liver, as well as kidney extraction is observed. This higher kidney uptake is also seen for peptides **1** and **20**, despite the structural differences between both peptides. The two peptide analogues containing the amide *N*-methyl groups (peptides **12** and **14**) present a more balanced distribution between the different organs. The serum levels observed 15 min after administration were the highest for peptide **1**, the lowest for peptide **9** and intermediate for peptides **10**, **12**, **14** and **20**.

***In vitro* metabolic stability—**The *in vitro* metabolic stability of unlabeled peptides **1** and **9** was determined in mouse plasma and brain homogenate using UPLC RP C18-chromatography, while the other peptides were investigated using the Prevail Organic Acid column (HPLC). All peptides could undeniably be distinguished from tissue-components, resulting in a reliable data evaluation. The peptides were observed to be very stable in mouse plasma and brain homogenate for at least two hours (Table 4). There is also no adsorption nor chemical degradation observed for the peptides under investigation. The BBB characteristics can thus be assigned to the native peptides. Comparatively, on the contrary, endomorphin-1 and endomorphin-2 for example show very poor half-lives in mouse plasma: a $t_{1/2}$ of 4-7 min indicates a rapid enzymatic degradation of these peptides.[28]

***In vivo* antinociceptive properties—**Given the superior potency of peptides **1** and **10** and the absence of promising *in vitro* affinity and potency data for the [Aba-Lys]- and [Aba-Nle]-containing peptides (compounds **16** to **19**), only the selected [Dmt^1]DALDA analogues **1**, **9**, **10**, **12**, **14** and **20** were investigated *in vivo* for their antinociceptive activity using the tail-flick test in mice, after intraperitoneal (i.p.) and subcutaneous (s.c.) administration. The antinociception, resulting from i.p. injection of the compounds, is shown in Figure 3, with morphine as a positive control. All peptides generated an antinociceptive effect significantly different from control mice receiving i.p. saline. As a reference peptide, the naturally occurring opioid peptide dermorphin (Tyr-D-Ala-Phe-Gly-Tyr-Pro-Ser-NH_2) was included in the study.[29] Figure 3 illustrates the inability of dermorphin to induce a significant antinociceptive effect at the applied dose after i.p. injection.

Peptide **9** had a relatively low antinociceptive activity, similar to morphine and dermorphin, at 60 min post i.p. injection. In contrast, the parent peptide **1** as well as the peptide bearing a D-Cit residue in position two (**10**) produced potent responses. Peptide **1** showed a maximum antinociceptive activity at 60 min post i.p. injection, while the maximum antinociceptive activity of peptide **10** was reached at an earlier time point, *i.e.* at 45 min. This can be explained by the lower initial K_{in} value together with the high serum concentration observed at 15 minutes post injection obtained for peptide **1**. Peptide **10** showed good initial brain influx properties, resulting in a relatively rapid onset of antinociception. The D-Arg^2→D-Cit^2 substitution changes the polarity of **1** in such a way that brain influx is accelerated (see K_{in} Table 2). The rapid relapse of antinociception, on the other hand, can be explained by the kidney and liver extraction, seen at 15 min post injection. Both peptides gave responses that were superior to the response of peptide **20.** Despite the high initial K_{in} value of peptide **20**, the efflux and kidney uptake characteristics highly influence its analgesic profile, as a slow and shallow antinociceptive response is produced by this peptide. Peptides **12** and **14** showed a rapid increase of antinociception over time, reaching the highest plateau values at 60-90 min post i.p. injection. During the first 45 min after injection, peptide **12** reached potent antinociception at a slower rate than peptide **14**. After the maximal effect, *i.e.* at the plateau decline phase, both peptides still showed a high antinociceptive activity (13 - 15 times higher than the antinociception of morphine). These analgesic profiles can be explained by the high initial brain influx properties (K_{in}) and insignificant outflux rate (k_{out}) of both peptides. Taken together, the relatively high serum concentrations after 15 min i.p. and the absence of massive tissue extraction, provide an explanation for the plateauing characteristics. Finally, the disappointing antinociceptive activity of peptide **9** can be understood by the low initial K_{in}, indicating a slow onset of antinociception, together with the excessive liver extraction results.

When analyzing the dose-normalized area under the curve values (AUCs, 1 μmol/kg) (Figure 3) of the initial 120 min post injection, we could conclude that peptide **14** (1412 %.min) had the highest antinociceptive effect, followed by peptide **12** (1187 %.min), peptide

1 (750 %.min), peptide **10** (521 %.min) and peptide **20** (253 %.min). The positive control morphine had a much lower AUC, *i.e.* 66 %.min, similar to peptide **9** (65 %.min) and dermorphin (46 %.min).

Looking at the structural characteristics of peptides **1**-**14**, it is clear that the C-terminal amino acid is the most determining factor for the antinociceptive activity: the presence of *N*MeLys (**12** and **14**) is preferred, followed by Lys (**1** and **10**), while other amino acids like Nle (**9**) decreased its antinociceptive activity significantly. The effect of varying Arg and Cit at position 2 is less pronounced, but cannot be neglected. It shows a confounding effect with the amino acid on position 4: if this is *N*MeLys, then Cit^2 gives a higher activity (**14** versus **12**), while if position 4 is Lys, the reverse is true and Arg^2 gives the highest activity (**1** versus **10**).

In addition to the primary evaluation of antinociceptive properties of peptides **1**, **9**, **10**, **12**, **14** and **20** after i.p. administration, a further *in vivo* study assessing the dose- and time-dependent antinociceptive effects after s.c. administration was performed using the mouse tail-flick test. Antinociceptive properties of the six peptides, given s.c., were compared to those of morphine and are illustrated in Figure 4. The calculated ED_{50} values with 95% confidence intervals are shown in Table 5. The overall profile of antinociceptive effects after s.c. administration closely match that determined after i.p. administration.

Dose-dependent and long duration of action lasting up to 6-7 h was shown by peptides **1** (Figure 4A), **12** (Figure 4D) and **20** (Figure 4F), while a shorter antinociceptive effect was produced by peptides **10** (Figure C) and **14** (Figure E) lasting about 2-3 h, still being longer than the effect of morphine. Compound **9** showed no dose-related antinociception, and failed to reach a 50% effect after s.c. administration of 6 μmol/kg (Figure 4B). All peptides, except **9**, were considerably more potent in eliciting an analgesic action than morphine (Figure 4 and Table 5).

In line with earlier reports,[11,12,30] [Dmt^1]DALDA **1** is a potent opioid antinociceptive agent when administered to mice s.c. in the tail-flick test, having a 44-fold increase in potency relative to morphine and a prolonged duration of action (Figure 4A). The high potency that characterizes [Dmt^1]DALDA **1** is, similarly to the i.p. administration, completely lost upon deletion of the Lys^4 side chain amino group resulting in analogue **9** (Figure 4B). On the contrary, compound **10** (Figure 4C), as well as its *N*MeLys^4 analogue **14** (Figure 4E), induce a potent effect with a peak at 1h. This observation clearly shows that only the removal of the Lys^4 side chain functionality is detrimental for antinociception. Following s.c. administration, peptide **12**, the *N*-methylated analogue of [$Dmt]^1$DALDA **1**, produced a prolonged antinociception action with a peak effect around 1-4 h and lasting up to 7 h (Figure 4D), a profile similar to that of the parent peptide. While it was equipotent to [$Dmt]^1$DALDA, compound **12** was about 51-fold more potent than morphine (Table 5). This finding was also true when comparing peptide **10** and its *N*-methyl analogue **14**, which show comparable potencies and similar time course of antinociceptive action in mice after s.c. administration, and an augmented potency relative to morphine. On this basis, *N*-methylation of the Lys residue in position 4 did not result in any major alterations in antinociceptive activities when injected s.c., while its replacement with Nle has a detrimental effect. Compound **20** also produced a significant antinociceptive action after s.c. administration with a peak effect at 1h (Figure 4F), but with a somewhat shorter duration of action than peptides **1** and **12**. It was 3- and 4-fold less potent in eliciting an antinociceptive effect, respectively. However, compared to morphine, peptide **20** still shows 14-fold increased analgesic potency after s.c. administration. Exchanging the D-Arg^2 residue in peptides **1** and **12** with a D-Cit residue, resulted in analogues **10** and **14**, respectively, which

retained high antinociceptive potency, while having a shorter duration of action (Figure 4C and 4E).

Altogether, the new peptidic [Dmt^1]DALDA analogues **10**, **12** and **14** emerged as potent antinociceptive agents after i.p. and s.c. administration, with several folds increased potency as compared to morphine. They differ in kinetic behavior, like BBB-characteristics and tissue distribution, resulting in different kinetic profiles of the antinociceptive activity.

Conclusions

From the substitution of the residues of [Dmt^1]-DALDA at position 2 and 4, by structurally related, but uncharged amino acids (*i.e.* D-Arg^2 by D-Cit^2 and Lys^4 by Nle^4), we conclude that side chain groups bearing the positive charges in [Dmt^1]DALDA are not needed for efficient *in vitro* receptor binding and activation. However, the removal of either side chain charges did diminish the well-established MOR subtype receptor selectivity of [Dmt^1]DALDA. Enhanced DOR binding was observed when one charge and even more when the two charges were eliminated. This trend was conserved throughout the 'parent' (**1** and **9** to **11**), the *N*-methylated (**12** to **15**) and the constrained "Aba" series (**16** to **19**). In regard to KOR affinity, the introduced modifications clearly had an impact on the binding affinity of the investigated peptides to this opioid receptor subtype. Low nanomolar KOR binding affinities were determined for peptide analogues **13**, **14**, **17** and **19** (with K^{κ}_{i} values between 1.12 and 14.4 nM). Because of the liabilities related to mu opioid analgesics such as morphine, ligands of KOR have also received considerable attention as potential analgesics.[31] In particular, KOR agonists have therapeutic potential in pain conditions associated with inflammation.

When looking at the transport properties of the peptide analogues in this study, all synthesized [Dmt^1]-DALDA peptides show influx into the brain parenchyma. The tissue distribution, on the other hand, indicated that the charged aminoalkyl chain of Lys^4 and the guanidine moiety of D-Arg^2, are of significant importance for the biodistribution of the peptides. Deletion of these charges, via D-Arg^2→D-Cit^2 and Lys^4→Nle^4 substitutions, decreases the 3+ net charge of the peptide, resulting in enhanced liver uptake, and potentially influences brain accessibility. As shown in this work, subtle structural modifications can influence the biodistribution of the peptide analogues and could lead to a modulated peptide delivery to the CNS, thus affecting the ratio of centrally vs. peripherally induced analgesia.

The ability of mice to sense a pain stimulus was verified after peripheral administration of a selection of opioid peptides. In contrast to the reference peptide [Dmt^1]DALDA **1**, which showed a very potent analgesic effect, the low antinociceptive effect of peptide **9** could be rationalized by a limited brain intake after massive liver extraction. Peptide **20** showed a rapid brain influx, but also a significant efflux, resulting in lower antinociception compared to the other peptides such as **1**, **12** and **14**.

Peptides **12** and **14** had the highest antinociceptive effect during the first 2h of an i.p. injection, measured as AUC relative to morphine (normalized at 1 μmol/kg), followed by peptides **1** and **10**. The presence of *N*MeLys^4 at the carboxyl terminus of the peptide sequence is thus preferred for antinociceptive activity, followed by Lys^4, while other amino acids like Gly^4 and Nle^4 significantly decreased the antinociception.

When the peptide analogues were investigated over a longer s.c. post-injection period (up to 7h) in a dose-dependency study, it became apparent that two distinct antinociception profiles were obtained. Comparable ED_{50} values were measured for peptides **1** and **12** (Dmt-D-Arg-Phe-(*N*Me)Lys-NH_2) in comparison with analogues **10** (H*Dmt-D-Cit-Phe-Lys-NH_2) and

14 (Dmt-D-Cit-Phe-(*N*Me)Lys-NH_2), but the latter peptides produced their peak effect more rapidly (1h vs. 2h post-injection for **1/12**). The steep increase in potency was also accompanied by a rapid decrease after reaching the maximum in antinociceptive effect. These observations are interesting for the development of peptide-based pharmaceuticals aiming at different pain types. Peptide **10** could serve as a lead molecule for the treatment of acute (e.g. post-operative pain), whereas the long-lasting Dmt-D-Arg-Phe-*N*MeLys-NH_2 **12** could be useful for addressing chronic pain conditions (e.g. neuropathic pain). As the compounds investigated in this study are potent dual MOR/DOR (and even KOR, see **17**) agonists, they could potentially be useful for the treatment of pain with reduced side effects and be effective at low administered doses.

Experimental section

General

Thin layer chromatography (TLC) was performed on plastic sheet pre-coated with silica gel $60F_{254}$ (Merck, Darmstadt, Germany) using specified solvent systems. Mass Spectrometry (MS) was recorded on a Micromass Q-Tof Micro spectrometer using electrospray (ESP) ionization (positive or negative ion mode). Data collection was done with Masslynx software. Analytical Reversed Phase (RP)-HPLC was performed using an Agilent 1100 Series system (Waldbronn, Germany) with a Supelco Discovery BIO Wide Pore® (Bellefonte, PA, USA) RP C-18 column (25 cm × 4.6 mm, 5 μm) using UV detection at 215 nm. The mobile phase (water/acetonitrile) contained 0.1% TFA. The gradient consisted of a 20 min run from 3 to 97% acetonitrile at a flow rate of 1mL/min. Preparative HPLC was performed on a Gilson apparatus and controlled with the software package Unipoint. The RP C18-column (Discovery BIO Wide Pore 25 cm × 21.2 mm, 10 μm) was used under the same conditions as the analytical RP-HPLC, but with a flow rate of 20 mL min^{-1}. A purity of more than 95% was determined for all compounds by analytical RP-HPLC using the conditions described above. ^{1}H-NMR and ^{13}C-NMR spectra were recorded at 250 MHz and 63 MHz, respectively, on a Bruker Avance 250 spectrometer or at 500 MHz and 125 MHz on a Bruker Avance II 500. Calibration was done with TMS (tetramethylsilane) or residual solvent signals as an internal standard. The solvent used is mentioned in all cases and the abbreviations used are: s (singlet), d (doublet), dd (double doublet), t (triplet), br s (broad singlet) and m (multiplet).

Opioid receptor binding assays

Opioid receptor binding studies were performed as described in detail elsewhere.[35] Binding affinities for MOR and DOR were determined by displacing, respectively, [^{3}H]DAMGO (Multiple Peptide Systems, San Diego, CA) and [^{3}H]DSLET (Multiple Peptide Systems) from rat brain membrane binding sites, and KOR receptor affinities were measured by displacement of [^{3}H]U69,593 (Amersham) from guinea pig brain membrane binding sites. Incubations were performed for 2 h at 0 °C with [^{3}H]DAMGO, [^{3}H]DSLET and [^{3}H]U69,593 at respective concentrations of 0.72, 0.78 and 0.80 nM. IC_{50} values were determined form log-dose displacement curves, and K_i values were calculated from the IC_{50} values by means of the equation of Cheng and Prusoff,[32] using values of 1.3, 2.6 and 2.9 nM for the dissociation constants of [^{3}H]DAMGO, [^{3}H]DSLET and [^{3}H]U69,593, respectively.

Functional GPI and MVD assays

The guinea pig ileum (GPI)[33] and mouse vas deferens (MVD)[34] bioassays were carried out as described in detail elsewhere.[35,36] A dose-response curve was determined with [Leu^{5}]enkephalin as standard for each ileum and vas preparation and IC_{50} values of the compounds being tested were normalized according to a published procedure.[37]

Blood-brain barrier transport

Animals—Male Institute for Cancer Research, Caesarean Derived-1 (ICR-CD-1) mice (Harlan Laboratories, Venray, The Netherlands), weighing 25-30 g, were used according to the Ethical Committee principles of laboratory animal welfare as approved by our institute (Ghent University, Faculty of Veterinary Medicine, 2009-052). Animals were housed under standard laboratory conditions in a temperature and humidity regulated environment with food and water ad libitum.

Reagents and peptides—Bovine serum albumin (BSA), calcium chloride dehydrate, D-glucose, HEPES, magnesium sulphate heptahydrate, potassium chloride, disodium hydrogen phosphate dihydrate, sodium dihydrogen phosphate monohydrate, sodium chloride, sodium lactate, urethane, and Krebs-Henseleit buffer were all purchased from Sigma (St. Louis, MO, USA) or Merck KGaA (Darmstadt, Germany). Dextran was obtained from AppliChem GmbH (Darmstadt, Germany), while dermorphin was purchased from Peptide Synthetics (PPR, Hampshire, United Kingdom). Morphine hydrochloride was acquired from Belgopia (Louvain-La-Neuve, Belgium).

Peptides ^{125}I radiolabeling—The Dmt^{1}-DALDA peptides and controls (dermorphin and BSA) were labeled by the Iodogen method.[37,39] Briefly, a 1 g/l peptide solution was prepared by dissolving about 1 mg in phosphate buffer (pH 7.4, 130 mM). A Iodo-Gen® coated tube was previously rinsed with 1 ml phosphate buffer. Subsequently, 50 μl NaI (20 nmol/10 μl) and 10 μl of Na^{125}I solution (3700 MBq/ml) (Perkin Elmer, Boston, MA, USA) were transferred into this Iodo-Gen® coated tube. After 6 min of incubation at room temperature, the oxidation reaction of iodide to iodonium was stopped by removing the solution from the tube and adding the iodonium solution to a tube containing 50 μl of peptide solution (1 μg/Kl). The iodination reaction of the peptide was allowed to proceed another 6 min at room temperature, after which the reaction mixture was purified with an Ag-filter. After Ag-purification, the radioactivity of the filtrate was measured using a dose calibrator (Veenstra, The Netherlands) to dilute the ^{125}I-peptide appropriately.

In addition, a quality control was performed on the filtrated peptide using a Vydac Everest C18 (250 mm × 4.6 mm I.D., 300 Å, 5 μm particle size) HPLC column (Grace Vydac, Hesperia, CA, USA) in an oven set at 30°C, with a mobile phase consisting of A) 0.1 % w/v formic acid in water, and B) 0.1 % w/v formic acid in acetonitrile. A linear gradient was employed as follows:

Peptide **1**: 0-50 min going from 98 % to 50 % A.

Peptides **9**, **12**, **14** and **20**: 0-40 min going from 98 % to 80 % A.

Peptide **10**: 0-40 min going from 98 % to 60 % A.

The flow rate was set at 1.0 ml/min with an injection volume of 100 μl.

The radio-HPLC apparatus consisted of a LaChrom Elite L-2130 pump with degasser, a LaChrom Elite L-2300 column oven, a LaChrom Elite L-2400 UV detector set at 215 nm (all Hitachi, Tokyo, Japan), a Rheodyne 7725i manual injector with 100 μl sample loop (Rheodyne, Rohnert Park, CA, USA) and a Berthold LB500 HERM radioactivity detector (Berthold Technologies, Bad Wildbad, Germany) equipped with EZChrom Elite version 3.1.7 software for data acquisition (Scientific Software, Pleasanton, CA, USA).

Multiple time regression (MTR)—In order to determine whether the peptides could enter the brain, multiple time regression analysis was performed. The CD-1 mice were

anesthetized with intraperitoneal (i.p.) urethane (3 g/kg) and the jugular vein and carotid artery were isolated. 200 μl of the radiolabeled peptides (30 000 cpm/μl) in Lactated Ringer's (LR) solution containing 1 % BSA were each injected separately into the jugular vein. At specified time points after injection, blood was obtained from the carotid artery and the mouse was decapitated. The brain was removed and weighed, after which radioactivity was determined in a gamma counter (Wallac Wizard automatic gamma counter, PerkinElmer, Shelton, CT, USA). The blood was centrifuged at 10 000 × *g* for 15 min at 21 °C and the radioactivity of the obtained serum was measured.

The theoretical background of the multiple time regression analysis is based on the Gjedde equation:[26]

$$\frac{A_m(t)}{C_p(t)} = K_{in}\frac{\int_0^t C_p(t)\cdot dt}{C_p(t)} + V_i$$

where $A_m(t)$ is the amount of radioactivity in brain at time t, $C_p(t)$ the amount of radioactivity in serum at time t, K_{in} the brain influx rate constant and V_i the initial brain distribution volume.

The exposure time (exp.t) is defined as the integral of the serum radioactivity over time divided by the radioactivity at time t: $exp.t = \frac{\int_o^t C_p(t)\cdot dt}{C_p(t)}$ The integral of the radioactivity over time is represented by the area under the curve (AUC).

Finally, the brain/serum ratios (μl/g) were plotted versus exposure time. The initial slope of the linear portion of this relationship over the first minutes measures the unidirectional initial influx rate (K_{in} initial) from blood to brain. The intercept represents the brain volume of distribution (V_{br}).

As a system suitability controls of this method, BSA, the impermeable vascular marker, as well as dermorphin, a weak positive influx control peptide,[28] were labeled with I-125 and their influx investigated as described above. In compliance with literature data,[40] a mean influx transfer constant of 0.0849 ± 0.0847 μl/(g × min) was obtained for BSA, confirming negligible influx. The mean K_{in} over 15 minutes for dermorphin was 0.173 ± 0.137 μl/(g × min), while the initial K_{in} was 5.52 ± 1.41 μl/(g × min) if the first minutes are considered, justifying its choice as a weak positive brain influx control.

Capillary depletion—This method was performed to determine to what extent the peptides, taken up by the brain, crossed the capillary wall instead of being trapped in the capillary cells. The method of Triguero et al.[41] as modified by Gutierrez et al.[42] was used. Summarizing, CD-1 mice were anesthetized with urethane (3 g/kg i.p.) and the jugular vein was isolated. 200 μl of the diluted peptide solution (10 000 cpm/μl) was injected in the jugular vein. At specified time points after injection, blood was collected from the abdominal aorta and the brain was perfused manually with 20 ml of LR buffer after severing the jugular veins. Subsequently, the brain was collected, homogenized with 0.7 ml of ice-cold capillary buffer (10 mM HEPES, 141 mM NaCl, 4 mM KCl, 2.8 mM $CaCl_2$, 1 mM $MgSO_4$, 1 mM NaH_2PO_4 and 10 mM D-glucose adjusted to pH 7.4) in a pyrex glass tube and mixed with 1.7 ml of 26 % ice-cold dextran solution in capillary buffer. The resulting solution was weighed and centrifuged in a swinging bucket rotor (Eppendorf, Hamburg, Germany) at 5400 × *g* for 30 min at 4 C. Pellet (capillaries) and supernatant (parenchyma and fat tissues) were collected, weighed and measured in a gamma counter. After

centrifuging the obtained blood, 50 μl of serum was collected and measured in a gamma counter. Compartmental BBB-distribution was evaluated from plotting capillaries/serum and parenchyma/serum activity ratios versus time.

Brain to blood transport—This method was performed to quantify the amount of peptide pumped out of the brain by efflux transport.[43] CD-1 mice were anesthetized with urethane (3 g/kg i.p.) and the skin of the skull was removed. A hole was then made into the lateral ventricle, 1 mm lateral and 0.34 mm posterior to the bregma, with a 22 G needle carrying a tubing guard at a constant depth of 2 mm. The anesthetized mice received an intracerebroventricular (i.c.v.) injection of 1 μl of LR solution containing the labeled peptide (25 000 cpm/μl) and 1 % BSA at a speed of 360 μl/h for 10 sec using a syringe pump (KDS100, KR analytical, Cheshire, UK). At specified time points after injection, blood was collected from the abdominal aorta and the mouse was decapitated. Subsequently, the whole brain was collected, weighed and measured in a gamma counter. The efflux rate constant k_{out} (min^{-1}) was calculated from the linear regression of the natural logarithm of the residual radioactivity in brain versus time, applying first order kinetics.

Tissue distribution—Immediately after brain collection, spleen, liver, lungs, heart and kidneys were collected.[44] Again, the tissues were weighed and measured in the gamma counter. For each tissue, the percentage of time-corrected injected dose (ID) was then calculated:

$$\text{Percentage}ID\,(\%) = \frac{\frac{A_{\text{tissue}}}{W_{\text{tissue}}}}{\frac{A_{\text{does injected}}}{W_{\text{animal}}}} \times 100$$

where A_{tissue} is the radioactivity of the tissue, w_{tissue} the weight of the tissue, $A_{dose\ injected}$ the amount of radioactivity injected into the vein and w_{animal} the body weight of the mouse.

***In vitro* metabolic stability—**In order to obtain information regarding the metabolic fate of peptides, the non-labeled peptides were tested *in vitro* by incubating in mouse plasma and mouse brain homogenate.[45] In brief, 100 μg of the non-labeled peptide dissolved in Krebs-Henseleit buffer (pH 7.4) was incubated in plasma or brain homogenate (250 μl of mouse plasma or 150 μg of tissue protein, *respectively*) at 37°C while shaking. At suitable time points, aliquots were taken and immediately transferred into microtubes containing 10 % v/v trifluoric acetic acid (TFA) solution in water to obtain a final concentration of 1:10 v/v solvent/aliquot. The samples were then heated for 5 min at 95°C, followed by cooling in an ice-bath for 30 min. After centrifugation of the samples at 15000 × *g* for 15 min at 5 °C, the supernatants were analyzed using UPLC-PDA and HPLC-UV. Placebos (mouse plasma or tissue homogenate), controls (initially inactivated tissue proteases) and reference solutions (peptide dissolved in buffer) were similarly processed. The time-dependent decrease of the native peptide was quantified and from the linear regression between the quantified decrease and time, the half-life ($t_{1/2}$) was determined as:

$$t_{\frac{1}{2}} = \frac{\ln(2)}{k}$$

where k is the first order rate constant.

If the calculated half-life was more than two times the experimental time, *i.e.* more than 4 hours, no quantitative half-life was given and the results expressed as “stable”.

UPLC-PDA analyses were performed using Waters Acquity H-Class Bio-samples FTN, a Waters Acquity H-Class BioQuaternary Solvent Manager, a Waters Acquity H-Class column module and a Waters Acquity H-Class Photodiode Array Detector (UV spectrum was recorded between 190 and 400 nm) equipped with Waters Empower Pro software version 2 (all Waters, Milford, MA, USA). Analysis was performed using a Waters Acquity UPLC BEH300 C18 column (100 × 2.1 mm I.D., 300 Å, 1.7 μm particle size) in an oven set at 35 °C. The following solvent system was used: A) 10 mM ammonium carbonate and B) acetonitrile. The gradient method consisted of a linear increase from 5 % B to 60 % B in 20 min, followed by 10 min reconditioning with initial composition 95/5 v/v A/B. The flow rate was set at 0.58 ml/min and the injection volume was 5 μl.

The degradation of the peptides was also studied by use of an HPLC system consisting of a Waters Alliance 2695 Separations module, a Waters column heater and a Waters 2487 Dual wavelength absorbance detector, fitted with Empower Pro software version 2 (all Waters, Milford, MA, USA). Quantification of the degradation was performed at 210 nm. Analysis was achieved using a Grace Alltech Prevail Organic Acid column (250 × 4.6 mm I.D., 110 Å, 5 μm particle size) in an oven set at 30 °C, using A) 25 mM phosphate buffer pH 8.0 and B) acetonitrile. The following linear gradient method was used: from 10% B to 70% B in 45 min, followed by 15 min with the initial composition (90/10 v/v A/B) to recondition the system. The flow rate was set at 1.0 ml/min with an injection volume of 20 μl.

Antinociceptive properties

A. After i.p. administration—The same type of mice as used for the BBB transport studies were used in this assay. Antinociception was assessed using the 55 °C tail withdrawal method in CD-1 mice. Each mouse (10 mice per group) was first tested for consistency in baseline latency by immersing its tail in the water and recording the time to response. Mice were then administered the controls as well as the test compounds at a dose of 5 mg/kg body weight and tested for antinociception at various time points afterwards. Antinociception was calculated as % antinociception or % MPE (percent maximum possible effect) using the following formula: 100 × (test latency – baseline latency) / (10 - baseline latency). To avoid tissue damage, a maximum score was assigned (100%) to animals that failed to respond within 10 s (=cut-off time).

A negative control consisted of a physiological 0.9 % saline solution. Two positive controls were also included, *i.e.* morphine and dermorphin, at a dose of 5 mg/kg. All controls were i.p. administered.

The amount of antinociception was determined using the AUC:

$$AUC=\sum_{i=1}^{n}\left(\frac{(y_i+y_{i-1})}{2}\times(x_i-x_{i-1})\right)$$

within the 120 min time points, y the percentage of antinociception and x the time after injection (min). Assuming first order kinetics, the AUC of the peptides and of morphine is converted to a theoretical AUC_p, *respectively* AUC_m, equivalent to a dose of 1 μmol active moiety/kg. The morphine normalized AUC for the peptides ($AUC_{normalized}$) is then calculated by:

$$AUC_{\text{normalized}}=\left(\frac{AUC_p}{AUC_m}\right)\times 100$$

B. After s.c. administration—Male CD-1 mice (25-35 g) were purchased from Charles River Laboratories (Sulzfeld, Germany). Animals were housed under standard laboratory conditions in a temperature-regulated environment under a controlled 12 h light/dark cycle with food and water ad libitum. All animal procedures were approved by the Austrian Ethical Committee on Animal Care and Use in line with international laws and policies.Morphine hydrochloride was obtained from Gatt-Koller GmbH (Innsbruck, Austria). All drugs were dissolved in sterile physiological saline (0.9%) and were administered s.c. in a volume of 10 μl per 1 g body weight.

The radiant heat tail-flick test was used to assess antinociceptive effects of tested drugs after s.c. administration in mice using an UB 37360 Ugo Basile analgesiometer (Ugo Basile s.r.l., Varese, Italy) as described.[46] The reaction time required by the mouse to remove its tail due to the radiant heat was measured and defined as the tail-flick latency. A cut-off time of 10 s was also used in order to minimize tissue damage, and the % antinociception or MPE for each dose administered was calculated as above. At least three doses were tested and five to six animals per dose were used. Antinociceptive ED_{50} values and 95% confidence limits were calculated by the method of Litchfield and Wilcoxon (1949).[47]

Compound Synthesis and characterization

Both Fmoc-Aba-Lys-OH **8a** and Fmoc-Aba-Nle-OH **8b** were prepared according to reported procedures (see supporting information).[23,24] Subsequently, all peptides were assembled as mentioned before by standard SPPS protocols employing Fmoc- or Boc-protected amino acid residues or dipeptides (**8a** and **8b**).

Peptide characterization

H-Dmt-D-Arg-Phe-Lys-NH_2 1—HPLC (standard gradient) : t_{ret} = 8.46 min. TLC R_f (EBAW) : 0.50 ; TLC R_f(BAW) : 0.24 ; ESI-HRMS [M+H$^+$] : m/z = 640.3950 (calculated for $C_{32}H_{48}H^+N_9O_5$: 640.3929)

H-Dmt-D-Arg-Phe-Nle-NH_2 9—HPLC (standard gradient) : t_{ret} = 10.57 min. TLC R_f (EBAW) : 0.62 ; TLC R_f(BAW) : 0.70 ; ESI-HRMS [M+H$^+$] : m/z = 625.3793 (calculated for $C_{32}H_{47}H^+N_8O_5$: 625.3820)

H-Dmt-D-Cit-Phe-Lys-NH_2 10—HPLC (standard gradient) : t_{ret} = 8.68 min. TLC R_f (EBAW) : 0.52 ; TLC R_f(BAW) : 0.35 ; ESI-HRMS [M+H$^+$] : m/z = 641.3759 (calculated for $C_{32}H_{47}H^+N_8O_6$: 641.3770)

H-Dmt-D-Cit-Phe-Nle-NH_2 11—HPLC (standard gradient) : t_{ret} = 11.06 min. TLC R_f (EBAW) : 0.72 ; TLC R_f(BAW) : 0.74 ; ESI-HRMS [M+H$^+$] : m/z = 626.3651 (calculated for $C_{32}H_{46}H^+N_7O_6$: 626.3661)

H-Dmt-D-Arg-Phe-*N*MeLys-NH_2 12—HPLC (standard gradient) : t_{ret} = 8.43 min. TLC R_f(EBAW) : 0.52 ; TLC R_f(BAW) : 0.24 ; ESI-HRMS [M+H$^+$] : m/z = 654.4064 (calculated for $C_{33}H_{50}H^+N_9O_5$: 654.4086)

H-Dmt-D-Arg-Phe-*N*MeNle-NH_2 13—HPLC (standard gradient) : t_{ret} = 10.67 min. TLC R_f(EBAW) : 0.62 ; TLC R_f(BAW) : 0.70 ; ESI-HRMS [M+H$^+$] : m/z = 639.3983 (calculated for $C_{33}H_{49}H^+N_8O_5$: 639.3977)

H-Dmt-D-Cit-Phe-*N*MeLys-NH_2 14—HPLC (standard gradient) : t_{ret} = 8.67 min. TLC R_f (EBAW) : 0.55 ; TLC R_f(BAW) : 0.37 ; ESI-HRMS [M+H$^+$] : m/z = 655.3915 (calculated for $C_{33}H_{49}H^+N_8O_6$: 655.3926)

H-Dmt-D-Cit-Phe-*N*MeNle-NH$_2$ 15—HPLC (standard gradient) : t_{ret} = 11.81 min. TLC R_f(EBAW) : 0.72 ; TLC R_f(BAW) : 0.74 ; ESI-HRMS [M+H$^+$] : m/z = 640.3823 (calculated for $C_{33}H_{48}H^+N_7O_6$: 640.3817)

H-Dmt-D-Arg-Aba-Lys-NH$_2$ 16—HPLC (standard gradient) : t_{ret} = 8.21 min. TLC R_f (EBAW) : 0.52 ; TLC R_f(BAW) : 0.24 ; ESI-HRMS [M+H$^+$] : m/z = 653.3913 (calculated for $C_{33}H_{48}H^+N_9O_5$: 652.3929)

H-Dmt-D-Arg-Aba-Nle-NH$_2$ 17—HPLC (standard gradient) : t_{ret} = 11.25 min. TLC R_f (EBAW) : 0.75 ; TLC R_f(BAW) : 0.74 ; ESI-HRMS [M+H$^+$] : m/z = 637.3826 (calculated for $C_{33}H_{47}H^+N_8O_5$: 637.3820)

H-Dmt-D-Cit-Aba-Lys-NH$_2$ 18—HPLC (standard gradient) : t_{ret} = 8.43 min. TLC R_f (EBAW) : 0.55 ; TLC R_f(BAW) : 0.32 ; ESI-HRMS [M+H$^+$] : m/z = 653.3794 (calculated for $C_{33}H_{47}H^+N_8O_6$: 653.3770)

H-Dmt-D-Cit-Aba-Nle-NH$_2$ 19—HPLC (standard gradient) : t_{ret} = 11.57 min. TLC R_f (EBAW) : 0.77 ; TLC R_f(BAW) : 0.74 ; ESI-HRMS [M+H$^+$] : m/z = 638.3659 (calculated for $C_{33}H_{46}H^+N_7O_6$: 638.3661)

H-Dmt-D-Arg-Aba-Gly-NH$_2$ 20—HPLC (standard gradient) : t_{ret} = 8.63 min. TLC R_f (EBAW) : 0.55 ; TLC R_f(BAW) : 0.45 ; ESI-HRMS [M+H$^+$] : m/z = 581.3220 (calculated for $C_{29}H_{39}H^+N_8O_5$: 581.3195)

Supplementary Material

Refer to Web version on PubMed Central for supplementary material.

Acknowledgments

The work of SB, DT and PWS was supported by a collaboration convention between the Ministère du Développement Economique, de l'Innovation et de l'Exportation du Québec and the Fund for Scientific Research – Flanders (FWO Vlaanderen) (PSR-SIIRI-417). SVD thanks the Institute for the Promotion of Innovation through Science and Technology in Flanders (IWT-Vlaanderen) for a PhD grant (No. 73402), and a Special Research Fund from the Ghent University (BOF) grant and mandate (No. 01J22510 and 01D38811) [EW, BDS, SS]. The research of PWS was also supported by grants CIHR (MOP-89716), and the NIH (DA-004443). MAC is supported by a NHMRC Australia Fellowship AF511105.

Abbreviations used

Aba	4-amino-1,2,4,5-tetrahydro-2-benzazepin-3-one
AUC	area under the curve value
BBB	blood-brain barrier
BSA	Bovine Serum Albumin
Cit	citrulline
CNS	central nervous system
DAMGO	[D-Ala^2,*N*MePhe^4,Gly-ol^5]enkephalin
Dmt	2′,6′-dimethyl-(*S*)-tyrosine
DOR	δ–opioid receptor

DSLET	[D-Ser^2,Leu^5]enkephalin-Thr^6
ESP	electrospray ionization mass-spectrometry
GPI	Guinea pig ileum
HEPES	4-(2-hydroxyethyl)-1-piperazineethanesulfonic acid
HOBt	1-hydroxybenzotriazole
ID	injected dose
i.p.	intraperitoneal
i.v.	intravenous
KOR	κ–opioid receptor
LR	Lactated Ringer's (solution)
k_{out}	brain efflux rate coefficient
MOR	μ–opioid receptor
MPE	maximal possible effect
MTR	Multiple time regression
MVD	mouse vas deferens
Nle	norleucine
NMM	N-methyl morpholine
K_{in}	unidirectional brain influx or uptake transfer constant
Pbf	2,2,4,6,7-pentamethyldihydrobenzofuran-5-sulfonyl
Phth	phthaloyl
RaNi	Raney Nickel
SAR	structure-activity relationship
s.c.	subcutaneous
SEM	standard error of the mean
TBTU	*O*-(Benzotriazol-1-yl)-*N,N,N',N'*-tetramethyluronium tetrafluoroborate
V_{br}	brain distribution volume
Z	benzyloxycarbonyl.

References

1. Horan P, Tallarida RJ, Haaseth RC, Matsunaga TO, Hruby VJ, Porreca F. Antinociceptive interactions of opioid delta receptor agonists with morphine in mice: supra- and sub-additivity. Life Sci. 1992; 50:1535–1541. [PubMed: 1315897]
2. He L, Lee NM. Delta Opioid Receptor Enhancement of Mu Opioid Receptor-induced Antinociception in Spinal Cord. J. Pharmacol. Exp. Ther. 1998; 285:1181–1186. [PubMed: 9618421]
3. Coop A, Rice KC. Role of delta-opioid receptors in biological processes. Drug News Perspect. 2000; 13:481–487. [PubMed: 12937621]
4. Schiller PW, Weltrowska G, Schmidt R, Nguyen TMD, Berezowska I, Lemieux C, Chung NN, Carpenter KA, Wilkes BC. Four different types of opioid peptides with mixed μ agonist/δ antagonist properties. Analgesia. 1995; 1:703–706.

5. Purington LC, Pogozheva ID, Traynor JR, Mosberg HI. Pentapeptides displaying mu opioid receptor agonist and delta opioid receptor partial agonist/antagonist properties. J. Med. Chem. 2009; 52:7724–7731. [PubMed: 19788201]
6. Purington LC, Sobczyk-Kojiro K, Pogozheva ID, Traynor JR, Mosberg HI. Development and in vitro characterization of a novel bifunctional mu-agonist/delta-antagonist opioid tetrapeptide. ACS Chem. Biol. 2011; 6:1375–1381. [PubMed: 21958158]
7. For discussion and literature overview of MOR agonists/DOR antagonists: Schiller PW. Bi- or multi-functional opioid peptide drugs. Life Sci. 2010; 86:598–603. [PubMed: 19285088] and references therein.
8. Schiller PW, Nguyen TMD, Berezowska I, Dupuis S, Weltrowska G, Chung NN, Lemieux C. Synthesis and in vitro opioid activity profiles of DALDA analogues. Eur. J. Med. Chem. 2000; 35:895–901. [PubMed: 11121615]
9. Szeto HH, Lovelace JL, Fridland G, Soong Y, Fasolo J, Wu D, Desiderio DM, Schiller PW. In vivo pharmacokinetics of selective mu-opioid peptide agonists. J. Pharm. Exp. Ther. 2001; 298:57–61.
10. Shimoyama M, Shimoyama N, Zhao GM, Schiller PW, Szeto HH. Antinociceptive and respiratory effects of intrathecal H-Tyr-D-Arg-Phe-Lys-NH_2 (DALDA) and [Dmt^1]-DALDA. J. Pharm. Exp. Ther. 2001; 297:364–371.
11. Neilan CL, Nguyen TMD, Schiller PW, Pasternak GW. Pharmacological characterization of the dermorphin analog [Dmt^1]DALDA, a highly potent and selective mu-opioid peptide. Eur. J. Pharmacol. 2001; 419:15–23. [PubMed: 11348625]
12. Zhao GM, Wu DL, Soong Y, Shimoyama M, Berezowska I, Schiller PW, Szeto HH. Profound spinal tolerance after repeated exposure to a highly selective mu-opioid peptide agonist: Role of delta-opioid receptors. J. Pharm. Exp. Ther. 2002; 302:188–196.
13. Sagan S, Karoyan P, Lequin O, Chassaing G, Lavielle S. N- and C-alfa methylation in biologically active peptides: Synthesis, structural and functional aspects. Curr. Med. Chem. 2004; 11:2799–2822. [PubMed: 15544477]

14a). Toniolo, C.; Goodman, M. Introduction to the Synthesis of Peptidomimetic. In: Goodman, M., editor. Methods of Organic Chemistry: Synthesis of Peptides and Peptidomimetics. Vol. vol E22c. Thieme, Stuttgart, New York: 2003. b) Hruby VJ, Li G, Haskell-Luevano C, Shenderovich M. Design of peptides, proteins and peptidomimetics in Chi space. Biopolymers. 1996; 43:219–266. [PubMed: 9277134] c) Grauer A, König B. Peptidomimetics - A versatile Route to Biologically Active Compounds. Eur. J. Org. Chem. 2009:5099–5111.

15. Ballet S, Feytens D, Buysse K, Chung NN, Tumati S, Keresztes A, Van Duppen J, Lai J, Varga F, Porreca F, Schiller PW, Vanden Broeck J, Tourwé D. Design of Novel Neurokinin 1 Receptor Antagonists Besed on Conformationally Constrained Aromatic Amino Acids and Discovery of a Potent Chimeric Opioid Agonist-Neurokinin 1 Receptor Antagonist. J. Med. Chem. 2011; 54:2467–2476. [PubMed: 21413804]
16. Ballet S, Feytens D, De Wachter R, De Vlaeminck M, Marczak ED, Salvadori S, de Graaf C, Rognan D, Negri L, Lattanzi R, Lazarus LH, Tourwé D, Balboni G. Conformationally Constrained Opioid Ligands: The Dmt-Aba and Dmt-Aia versus Dmt-Tic Scaffold. Bioorg. Med. Chem. Lett. 2009; 19:433–437. [PubMed: 19062273]
17. Tourwé D, Verschueren K, Frycia A, Davis P, Porreca F, Hruby VJ, Toth G, Jaspers H, Verheyden P, Van Binst G. Conformational restriction of Tyr and Phe side chains in opioid peptides: Information about preferred and bioactive side3chain topology. Biopolymers. 1996; 38:1–12. [PubMed: 8679939]
18. Ballet S, Frycia A, Piron J, Chung NN, Schiller PW, Kosson P, Lipkowski AW, Tourwé D. Synthesis and biological evaluation of constrained analogues of the opioid peptide H-Tyr-D-Ala-Phe-Gly-NH_2 using the 4-amino-2-benzazepin-3-one scaffold. J. Pept. Res. 2005; 66:222–230. [PubMed: 16218989]
19. Guillemyn K, Kleczkowska P, Novoa A, Vandormael B, Van den Eynde I, Kosson P, Asim MF, Schiller PW, Spetea M, Lipkowski AW, Tourwé D, Ballet S. In vivo antinociception of potent mu opioid agonist tetrapeptide analogues and comparison with a compact opioid agonist – NK1 receptor antagonist chimera. Mol. Brain. 2012; 5:4. [PubMed: 22289619]

20a). Weltrowska G, Berezowska I, Lemieux C, Chung NN, Wilkes BC, Schiler PW. N-methylated cyclic analogues retain high opioid receptor binding affinity. Chem. Biol. Drug. Des. 2010;

75:182–188. [PubMed: 20028398] b) Hansen, PE.; Morgan, BA. Structure-activity relationships in enkephalin peptides. In: Udenfriend, S.; Meienhofer, J., editors. The peptides: Analysis, Synthesis, Biology. Vol. vol. 6, "Opioid peptides: Biology, chemistry and egentics. Academic Press; Orlando, USA: p. 269-321.

21. Ballet S, Misicka A, Kosson P, Lemieux C, Chung NN, Schiller PW, Lipkowski AW, Tourwé D. Dermorphin Tetrapeptide Analogues: Role of Lipophilicity vs. Structural Flexibility. J. Med. Chem. 2008; 51:2571–2574. [PubMed: 18370374]
22. Vandormael B, Fourla D-D, Gramowski-Vaz A, Kosson P, Weiss DG, Schröder OH-U, Lipkowski AW, Georgoussi Z, Tourwé D. Superpotent [Dmt1]Dermorphin Tetrapeptides Containing the 4-Aminotetrahydro-2-benzazepin-3-one Scaffold with Mixed m/d Opioid Receptor Agonistic Properties. J. Med. Chem. 2011; 54:7848–7859. [PubMed: 21978284]
23. Van Rompaey K, Van den Eynde I, De Kimpe N, Tourwé D. A versatile synthesis of 2-substituted 4-amino-1,2,4,5-tetrahydro-2-benzazepine-3-ones. Tetrahedron. 2003; 59:4421–4432.
24. Ballet S, Mayorov A, Cai M, Tymecka D, Chandler KB, Palmer ES, Van Rompaey M, Misicka A, Tourwé D, Hruby VJ. Novel selective human melanocortin-3 receptor ligands: Use of the 4-amino-1,2,4,5-tetrahydro-benzazepin-3-one (Aba) scaffold. Bioorg. Med. Chem. Lett. 2007; 17:2492–2498. [PubMed: 17314042]
25. Casimir JR, Guichard G, Briand JP. Methyl 2-((succinimidooxy)carbonyl)benzoate (MSB): A new, efficient reagent for N-phthaloylation of amino acid and peptide derivatives. J. Org. Chem. 2002; 67:3764–3768. [PubMed: 12027691]
26. Gjedde A. High-affinity and low-affinity transport of d-glucose from blood to brain. J. Neurochem. 1981; 36:1463–1471. [PubMed: 7264642]
27. Van Dorpe S, Adriaens A, Polis I, Peremans K, Van Bocxlaer J, De Spiegeleer B. Analytical characterization and comparison of the blood-brain barrier permeability of eight opioid peptides. Peptides. 2010; 31:1390–1399. [PubMed: 20347901]
28. Van Dorpe S, Adriaens A, Vermeire S, Polis I, Peremans K, De Spiegeleer B. Desirability function combining metabolic stability and functionality of peptides. J. Pept. Sci. 2011; 17:398–404. [PubMed: 21294224]
29. Van Dorpe S, Bronselaer A, Nielandt J, Stalmans S, Wynendaele E, Audenaert K, Van De Wiele C, Burvenich C, Peremans K, Hsuchou H, De Tré G, De Spiegeleer B. Brainpeps: the blood-brain barrier peptide database. Brain Struct Funct. 2012 DOI: 10.1007/s00429-011-0375-0.
30. Riba P, Ben Y, Nguyen T.M.y, Furst S, Schiller PW, Lee NM. [Dmt^1]DALDA is highly selective and potent at mu opioid receptors, but is not cross3tolerant with systemic morphine. Curr. Med. Chem. 2002; 9:31–39. [PubMed: 11860345]
31. Aldrich JV, McLaughlin JP. Peptide Kappa Opioid Receptor Ligands: Potential for Drug Development. AAPS J. 11:312–322. [PubMed: 19430912]
32. Cheng YC, Prusoff WH. Relationship Between the Inhibition Constant (Ki) and the Concentration of Inhibitor Which Causes 50 per cent (I_{50}) of an Enzymatic Reaction. Biochem.Pharmacol. 1973; 22:3099–3108. [PubMed: 4202581]
33. Paton WDM. The Action of Morphine and Related Substances on Contraction and on Acetylcholine Output of Coaxially Stimulated Guinea-pig ileum. Br. J. Pharmacol. Chemother. 1957; 12:119–127. [PubMed: 13413163]
34. Henderson G, Hughes J, Kosterlitz HW. A New Example of a Morphine-Sensitive Neuro-Effector Junction: Adrenergic Transmission in the Mouse Vas Deferens. Br. J. Pharmacol. 1972; 46:764–766. [PubMed: 4655272]
35. Schiller PW, Lipton A, Horrobin DF, Bodansky M. Unsulfated C-Terminal 7-Peptide of Cholecystokinin: A New Ligand of the Opiate Receptor. Biochem. Biophys. Res Commun. 1978; 85:1332–1338. [PubMed: 217386]
36. DiMaio J, Nguyen TMD, Lemieux C, Schiller PW. Synthesis and Pharmacological Characterization in Vitro of Cyclic Enkephalin Analogues: Effect of the Conformational Constraints on Opioid Receptor Selectivity. J. Med. Chem. 1982; 25:1432–1438. [PubMed: 6296388]

37. Waterfield AA, Leslie FM, Lord JAH, Ling N, Kosterlitz HW. Opioid Activities of Frangments of β-Endorphin and Its Leucine^5-Analogue. Comparison of the Binding Properties of Methionine- and Leucine-Enkephalin. Eur. J. Pharmacol. 1979; 58:11–18. [PubMed: 499333]
38. Vergote V, Baert B, Vandermeulen E, Peremans K, Van Bree H, Slegers G, Burvenich C, De Spiegeleer B. LC-UV/MS characterisation and DOE optimization of the iodinated peptide obestatin. J. Pharm. Biomed. Anal. 2008; 46:127–136. [PubMed: 18024048]
39. Vergote V, Bode S, Peremans K, Van Bree H, Baert B, Slegers G, Burvenich C, De Spiegeleer B. Analysis of iodinated peptides by LC-DAD/ESI ion trap mass spectrometry. J. Chromat.B. 2007; 850:213–220.
40. Kastin AJ, Akerstrom V. Entry of exendin-4 into brain is rapid but may be limited at high doses. Int. J. Obesity. 2003; 27:313–318.
41. Triguero D, Buciak J, Pardridge WM. Capillary depletion method for quantification of blood-brain-barrier transport of circulating peptides and plasma-proteins. J. Neurochem. 1990; 54:1882–1888. [PubMed: 2338547]
42. Gutierrez EG, Banks WA, Kastin AJ. Murine tumor-necrosis-factor-alpha is transported from blood to brain in the mouse. J. Neuroimmunol. 1993; 47:169–176. [PubMed: 8370768]
43. Banks, WA.; Kastin, AJ.; Conn, PM. Methods in Enzymology. Vol. Volume 168. Academic Press; 1989. Quantifying carrier-mediated transport of peptides from the brain to the blood; p. 652-660.
44. Czihal P, Knappe D, Fritsche S, Zahn M, Berthold N, Piantavigna S, Müller U, Van Dorpe S, Herth N, Binas A, Köhler G, De Spiegeleer B, Martin LL, Nolte O, Sträter N, Alber G, Hoffman R. ACS Chem. Biol. DOI: 10.1021/cb300063v, Publication date (Web): May 17, 2012.
45. Svenson J, Vergote V, Karstad R, Burvenich C, Svendsen JS, De Spiegeleer B. Metabolic Fate of Lactoferricin-Based Antimicrobial Peptides: Effect of Truncation and Incorporation of Amino Acid Analogs on the In Vitro Metabolic Stability. J. Pharmacol. Exp.Ther. 2010; 332:1032–1039. [PubMed: 19952307]
46. Spetea M, Bohotin CR, Asim MF, Stübegger K, Schmidhammer H. In vitro and in vivo pharmacological profile of the 5-benzyl analogue of 14-methoxymetopon, a novel μ opioid analgesic with reduced propensity to alter motor function. Eur. J. Pharm. Sci. 2010; 41:125–135. [PubMed: 20600882]
47. Litchfield JT Jr, Wilcoxon F. A simplified method of evaluating dose-effect experiments. J. Pharmacol. Exp. Ther. 1949; 96:99–113. [PubMed: 18152921]

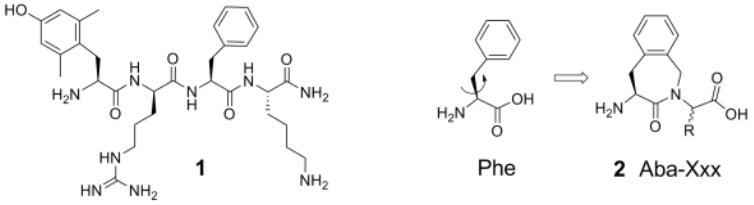

Figure 1.

Structures of Dmt-DALDA **1**, Phe and the conformationally constrained 4-amino-1,2,4,5-tetrahydro-2-benzazepin-3-one (Aba)-containing dipeptide **2** (with Xxx: an α-amino acid residue).

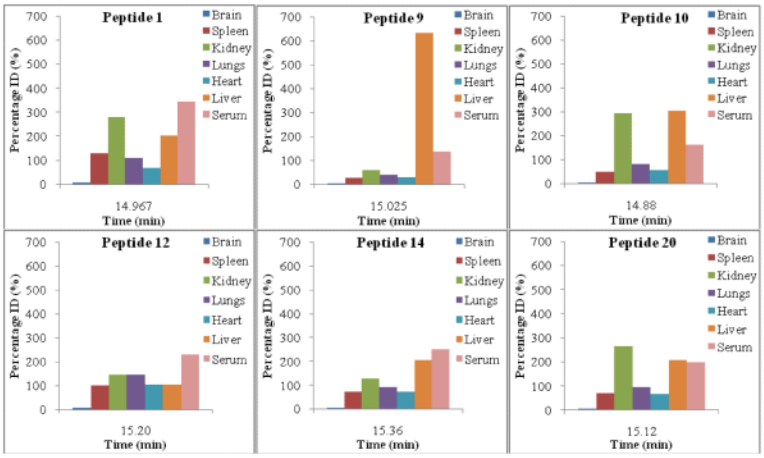

Figure 2.
Mean distribution of the [^{125}I]-peptides into the different tissues.

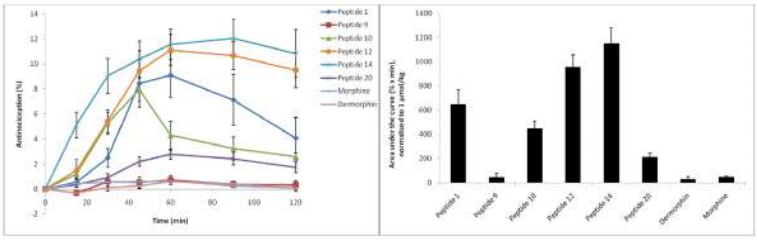

Figure 3.

Antinociceptive characteristics of the [Dmt[1]]-DALDA analogues after i.p. administration. **Left:** Time response curves of the peptides (dose of 1 μmol/kg, n = 10). Morphine and dermorphin at a dose of 1 μmol/kg (n = 10) were used as positive controls. The error bars represent the standard error of the mean (SEM). All data were saline-corrected. **Right:** Area under the curve normalized to a dose of 1 μmol/kg, based on antinociception measured during 120 min post-injection.

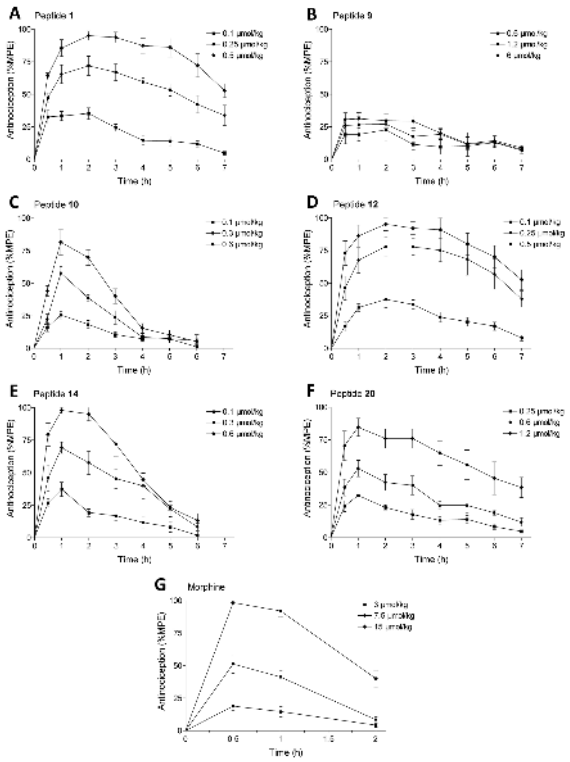

Figure 4.

Antinociceptive activities of peptides **1**, **9**, **10**, **12**, **14** and **20** and morphine after s.c. administration in the mouse tail-flick test. Dose- and time-dependent antinociceptive response presented as %MPE. Data are shown as mean ± SEM.

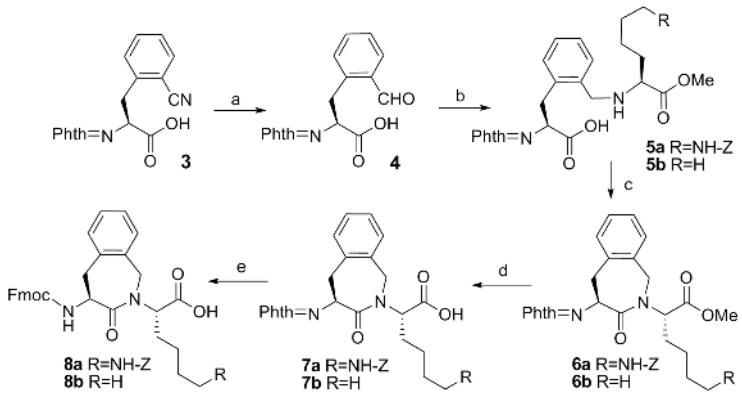

Scheme 1.

Synthesis of Fmoc-Aba-Lys(Z)-OH **8a** and Fmoc-Aba-Nle-OH **8b** dipeptide mimetics. Reaction conditions: a) H_2 (50 psi), RaNi, H_2O/AcOH/Py 1:1:1, 50°C, 38h, 78%; b) 1.1 eq HCl.H-Lys(Z)-OMe or HCl.H-Nle-OMe, 2.5 eq. $NaCNBH_3$, 20wt% $MgSO_4$, CH_2Cl_2, NMM or AcOH, r.t., 14h; c) 1.1. eq. DCC, Py, CH_3CN/ H_2O 1:1, r.t., 14h; d) acetone/HCl 1N 1:1, r.t., reflux, 16h; e) i. 4 eq. $NH_2NH_2.H_2O$, EtOH, reflux, 1.5h and ii. 1.2 eq. Fmoc-OSu, 2.2 eq. $NaHCO_3$, acetone/water 1:2, r.t, 2h.

Table 1

Structures, receptor MOR/DOR binding affinities and *in vitro* potency data

Structure	Comp.	MOR K_i (nM) [c]	DOR K_i (nM) [c]	KOR K_i (nM)	K_i ratio μ/δ/κ	GPI (μ) IC_{50} (nM) [c]	MVD (δ) IC_{50} (nM) [c]
H-Dmt-D-Arg-Phe-Lys-NH_2 [d]	**1**	0.143	2100	22.3	1/11400/156	1.41	23.1
H-Dmt-D-Arg-Phe-Nle-NH_2	**9**	0.23	15.2	16.2	1/66/70	2.2	6.2
H-Dmt-D-Cit-Phe-Lys-NH_2	**10**	0.57	50.0	20.9	1/88/37	0.31	1.4
H-Dmt-D-Cit-Phe-Nle-NH_2	**11**	0.79	3.98	98.5	1/5/125	0.89	4.7
H-Dmt-D-Arg-Phe-*N*MeLys-NH_2	**12**	0.26	309	56.1	1/1190/216	8.3	7.0
H-Dmt-D-Arg-Phe-*N*MeNle-NH_2	**13**	0.26	16.0	14.4	1/62/55	4.35	1.5
H-Dmt-D-Cit-Phe-*N*MeLys-NH_2	**14**	0.94	39.2	11.5	1/42/12	1.01	4.4
H-Dmt-D-Cit-Phe-*N*MeNle-NH_2	**15**	2.92	5.03	>10.000	1/2/>3420	0.65	1.5
H-Dmt-D-Arg-Aba-Lys-NH_2	**16**	0.61	38.6	ND	1/64/-	76.0	64 (IC_{25})
H-Dmt-D-Arg-Aba-Nle-NH_2	**17**	0.43	7.46	1.12	1/17/3	1.45	3.1
H-Dmt-D-Cit-Aba-Lys-NH_2	**18**	2.62	56.9	ND	1/22/-	49.0	1000
H-Dmt-D-Cit-Aba-Nle-NH_2	**19**	0.93	3.18	11.1	1/3/12	0.78 (IC_{35})	1.16
H-Dmt-D-Arg-Aba-Gly-NH_2 [e]	**20**	0.15	0.60	118	1/4/787	0.32	0.42

[c] Values represent means of 3-6 experiments. The GPI functional assay is representative of MOR activation, whereas the MVD is a DOR receptor-representative assay. Binding affinities of compounds for MOR and DOR opioid receptors were determined by displacement of [^{3}H]DAMGO ([D-Ala^2,NMePhe^4,Gly-ol^5]enkephalin) and [^{3}H]DSLET ([D-Ser^2,Leu^5]enkephalin-Thr^6) from rat brain membrane binding sites, respectively. KOR receptor binding affinities were determined by displacement of [^{3}H]U69,593 from guina pig ileum membrane binding sites.

[d] Data taken from ref.8,

[e] Data taken from ref.15

Table 2

Blood-brain barrier transport data of the [^{125}I]-peptides (mean ± SEM).

Peptide	K_{in} initial (μl/(g×min))	V_{br} (μl/g)	Capillary fraction (%)	Parenchyma fraction (%)	k_{out} (min^{-1})
1	9.44 ± 0.41	19.25 ± 1.02	23.12 ± 10.26	76.88 ± 10.26	0.058 ± 0.11
9	8.48 ± 1.61	27.43 ± 4.80	32.97 ± 9.99	67.03 ± 9.99	−0.039 ± 0.11
10	14.91 ± 0.10	27.12 ± 3.76	19.39 ± 15.81	80.61 ± 15.81	0.027 ± 0.022
12	18.11 ± 0.78	21.99 ± 2.81	25.95 ± 0.95	74.05 ± 0.95	0.028 ± 0.030
14	11.35 ± 0.61	17.13 ± 2.36	21.84 ± 1.32	78.16 ± 1.32	0.010 ± 0.038
20	14.89 ± 1.34	24.01 ± 3.41	30.95 ± 19.75	69.05 ± 19.75	0.096 ± 0.046

Table 4

Peptide recovery after 2 hours of *in vitro* incubation

Peptide	Mean recovery in plasma (%)	Mean recovery in brain (%)
1	94.7	102.6
9	90.2	103.7
10	98.3	96.2
12	112.4	94.0
14	103.9	95.0
20	107.2	99.6

Table 5

Antinociceptive potencies of peptides **1**, **9**, **10**, **12**, **14** and **20** in comparison to morphine after s.c. administration in the mouse tail-flick test

Compound	ED_{50} μmol/kg (95% confidence limits)[a]	Relative potency to Morphine
1	0.15 (0.07-0.32)	44
9	>6	n.d.
10	0.23 (0.10-0.55)	29
12	0.13 (0.06-0.30)	51
14	0.16 (0.07-0.36)	41
20	0.47 (0.18-1.2)	14
Morphine	6.6 (3.5-12.6)	1

[a] ED_{50} was determined at the time of peak effect (*i.e.* 2 h for peptide **1** and **12**, 1h for peptides **10**, **14**, and **20** and 30 min for morphine). n.d.: not determined.